A simple explicit thermodynamic closure for multi-fluid simulations including complex vapor-liquid equilibria: application to NH 3 -H 2 O mixtures

J. Carmona, I. Raspo, V. Moureau, P. Boivin

A simple explicit thermodynamic closure for multi-fluid simulations including complex vapor-liquid equilibria: application to $NH_3 - H_2O$ mixtures.

J. Carmona[1a], I. Raspo[b], V. Moureau[a], P. Boivin[b]

[a] *CORIA, CNRS UMR6614, Normandie Université, UNIROUEN, INSA of Rouen, France*

[b] *Aix Marseille Univ, CNRS, Centrale Med, M2P2, Marseille, France*

Abstract

This paper presents a new thermodynamic closure formulation appropriate for the simulation of subcritical multiphase flows, where two liquid/vapor components need to be considered, in addition of an arbitrary number of perfect gas non-condensable components. Assuming each component to follow the Noble-Abel Stiffened Gas (NASG) equation of state allows to derive a fully explicit formulation for the mixture pressure. A matching phase transition solver is then proposed, to compute efficiently and accurately the thermochemical equilibrium of the said mixture. The model capabilities are then illustrated through a two-dimensional simulation of a liquid ammonia tank leak into 80%-saturated humid air, where water is found to significantly condensate when interacting with the ammonia jet.

Keywords: Computational fluid dynamics, Multiphase compressible flow, Diffuse interface method, Vapor-Liquid phase transition, Thermodynamic equilibrium, Equation of state, Leakage, Pressurized liquefied gas

[1]Corresponding author: `julien.carmona@coria.fr`

1. Introduction

Alternative to hydrocarbons for transport and energy applications are being actively investigated, in line with world-wide decarbonization objectives. Hydrogen H_2 is an interesting energy carrier candidate, with the highest specific energy among fuels. Its low volumetric energy density brings safety issues [1] for transport applications, where space is a constraint: H_2 then either needs to be heavily compressed to 700-900 bars, or cooled to cryogenic temperatures for tanks to have a reasonable size.

Ammonia NH_3 may present an interesting compromise [2]: the molecule has a volumetric energy density higher than that of H_2, and is found liquid for much more moderate conditions, 4-10 bar at ambient temperature, compared to cryogenic H_2.

Whether liquid H_2 and/or NH_3 is retained as energy carrier, complex phase transition problems are encountered in the design of the storage systems. For both fuels, the saturation temperature is significantly lower than that of water, so any leak from the system will trigger condensation, or even freezing of the water contained in the surrounding air. This phase change is important to take into account, as water concentration has a significant impact, e.g. on reactivity [3, 4].

In the presence of two liquid (or condensable) phases, the Vapor-Liquid Equilibria (VLE) are complex since two components of the mixture are involved. Then, the equality of chemical potentials of both species in vapor and liquid phases must be prescribed. This equilibrium condition is usually expressed in terms of fugacity, especially when an Equation of State (EoS)

is used. However, depending on the pressure and temperature range of interest, simplifications can be done. At low and moderate pressure, the vapor phase can be considered as a perfect gas and the fugacity is replaced by the component partial pressure. Moreover, if the liquid phase is supposed to be an ideal solution, the equilibrium condition can be replaced by the very simple Raoult's law. An intermediate solution is provided by the generalized Raoult's law, used in the present paper, where the Poynting factor and the activity coefficient are introduced to account for the non-ideality of the mixture. The activity coefficient is then obtained from a Gibbs free energy model, such as Wilson, UNIQUAC, UNIFAC or NRTL models [5]. Whatever the model used or the assumptions made, the coupling of the VLE condition with the mass balance leads to the well-known Rachford-Rice Eq. (18).

Solving multi-component VLE coupled with fluid simulations may therefore be costly since the computation typically has to be performed at every grid point and time step. Diminishing this cost can be achieved via tabulation of the VLE over a range of conditions [6]. While table lookup is inexpensive when few input parameters are needed, table generation may however require significant resources, especially when the range of interest is wide. When only one constituent is condensable, a variety of phase transition model are available [7–13], but none of them – to the authors knowledge – is valid when two components in the liquids are present. The present study aims at bridging this gap.

The present study has two main objectives, answered in the first two sections of this paper. First, a new explicit thermodynamic closure is provided for mixtures consisting of two miscible liquid-vapor couples as well as an ar-

bitrary number of non-condensable gases. Second, a dedicated simple VLE solver is derived, for use in numerical simulations.

Canonical validations are presented in Sec. 4. They are carried out in the context of a multi-fluid 4-equation model [10, 11, 14–18] – which is derived from the 7-equation Baer–Nunziato model [19] by assuming instantaneous mechanical and thermal relaxation – but the VLE model is flow solver independent. Finally, an ammonia tank leak into humid air is investigated in Sec. 5, evidencing the presence of water condensation in the vicinity of the NH_3 jet.

2. Multiphase thermodynamic closure

2.1. The Noble-Abel Stiffened-Gas equation of state

The thermodynamic closure for a multiphase mixture is based on the Noble-Abel Stiffened Gas (NASG) EoS for each of its constituents:

$$p(\rho, T) = \frac{\rho(\gamma - 1)C_v T}{(1 - \rho b)} - p_\infty, \tag{1}$$

where p is the pressure, ρ is the density, T is the temperature, γ is the heat capacity ratio, C_v is the specific heat capacity at constant volume (or at constant pressure, $C_p = \gamma C_v$), b is the covolume, and p_∞ is a parameter representing the molecular attraction in the liquid phase. In this study, coefficients γ, C_v, b and p_∞ are assumed to be constant [20].

Considering a mixture of N constituents, each component is identified by the subscript $k = 1, ..., N$ and its thermodynamic state is denoted as $\phi = l$ for liquid or $\phi = g$ for gas. For each k component in a state ϕ, specific volume $v_{k,\phi}$, specific enthalpy $h_{k,\phi}$, specific internal energy $e_{k,\phi}$ and sound speed $c_{k,\phi}$

read:

$$\begin{cases} v_{k,\phi}(p,T) = \dfrac{(C_{p,k,\phi} - C_{v,k,\phi})T}{p + p_{\infty,k,\phi}} + b_{k,\phi} \\ h_{k,\phi}(p,T) = C_{p,k,\phi}\, T + b_{k,\phi} p + q_{k,\phi}, \\ e_{k,\phi}(p,T) = \dfrac{p + \gamma_{k,\phi}\, p_{\infty,k,\phi}}{p + p_{\infty,k,\phi}} C_{v,k,\phi}\, T + q_{k,\phi}, \\ c^2_{k,\phi}(p,T) = \dfrac{\gamma_{k,\phi}\, v^2_{k,\phi}\, (p + p_{\infty,k,\phi})}{v - b_{k,\phi}}, \end{cases} \tag{2}$$

where $q_{k,\phi}$ is the reference energy (here at $T = 0$ K).

The saturation pressure $p_{sat,k}(T)$ for the condensable components may be computed by an iterative procedure solving the equality of the chemical potentials as in [21] or by simple Antoine correlations as suggested in [20]. Saturation properties computations being extensively required, the latter is chosen here in order to get an explicit calculation. Antoine's parameters as well as their range of validity are given in Sec. 3.3 for the components of interest.

2.2. Equation of state for the mixture

In the following, mechanical and thermal equilibria are assumed in the elemental volume. The flow is thus locally represented as a mixture where each component shares a common pressure, velocity and temperature, but occupies its own sub-volume [15]. As an example, Fig. 1 represents an elemental volume consisting of two miscible liquid-vapor couples of species and an arbitrary number of non-condensable gases at mechanical and thermal equilibria. As each sub-volume is at the same pressure and temperature, the mixture specific volume and internal energy are linked to (p, T) by the

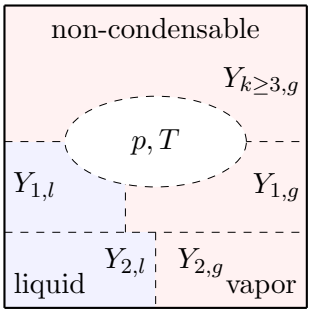

Figure 1: Representation of a control volume containing two miscible liquid-vapor couples of species and an arbitrary number of non-condensable gases at mechanical and thermal equilibria.

following mixture relations:

$$\begin{cases} v &= \sum_{k=1}^{N} \sum_{\phi=l,g} Y_{k,\phi}\, v_{k,\phi}(p,T), \\ e &= \sum_{k=1}^{N} \sum_{\phi=l,g} Y_{k,\phi}\, e_{k,\phi}(p,T), \end{cases} \tag{3}$$

where $Y_{k,\phi}$ is the mass fraction of the k^{th} constituent at ϕ state.

For use in a conservative solver [11, 15, 20, 22], temperature T and pressure p must be expressed as functions of the conservative variables. It is then necessary to invert system (3).

To that intent, temperature may be expressed from (3) by:

$$T = \frac{v - \bar{b}}{\sum_{k=1}^{N} \sum_{\phi=l,g} \frac{Y_{k,\phi}(\gamma_{k,\phi}-1)C_{v,k,\phi}}{p+p_{\infty,k,\phi}}}, \tag{4}$$

with $\bar{b} = \sum_{k=1}^{N} \sum_{\phi=l,g} Y_{k,\phi} b_{k,\phi}$. Alternatively, T may be obtained as a function of the mixture energy as:

$$T = \frac{e - \bar{q}}{\sum_{k=1}^{N} \sum_{\phi=l,g} Y_{k,\phi} C_{v,k,\phi} \left(\frac{p+\gamma_{k,\phi} p_{\infty,k,\phi}}{p+p_{\infty,k,\phi}} \right)}, \tag{5}$$

with $\bar{q} = \sum_{k=1}^{N} \sum_{\phi=l,g} Y_{k,\phi}\, q_{k,\phi}$.

Further assuming that the mixture is composed of only two condensable components ($k = 1, 2$) and any number of non-condensable gases and that $\forall k = 1, ..., N$, $p_{\infty,k,g} = 0$ – i.e. that for $k = 1, ..., N$ and $\phi = g$ the constituent k obeys the Clausius-Clapeyron EoS for gases – equality of expressions (4) and (5) leads to a cubic equation for p as a function of (v, e):

$$a_3 p^3 + a_2 p^2 - a_1 p - a_0 = 0, \tag{6}$$

with

$$\begin{cases} a_0 = p_{\infty,1,l}\, p_{\infty,2,l} \sum_{k=1}^{N} Y_{k,g} C_{v,k,g} A_{k,g} \\ a_1 = \sum_{k=1}^{N} \sum_{\phi=l,g} Y_{k,\phi} C_{v,k,\phi} A_{k,\phi} (\bar{p}_\infty - p_{\infty,k,\phi}) - p_{\infty,1,l}\, p_{\infty,2,l} \sum_{k=1}^{N} Y_{k,g} C_{v,k,g} \\ a_2 = \sum_{k=1}^{N} \sum_{\phi=l,g} Y_{k,\phi} C_{v,k,\phi} (\bar{p}_\infty - p_{\infty,k,\phi} - A_{k,\phi}) \\ a_3 = \sum_{k=1}^{N} \sum_{\phi=l,g} Y_{k,\phi} C_{v,k,\phi}, \end{cases} \tag{7}$$

$$\bar{p}_\infty = \sum_{k=1}^{N} p_{\infty,k,l} = p_{\infty,1,l} + p_{\infty,2,l} \tag{8}$$

and

$$A_{k,\phi} = (\gamma_{k,\phi} - 1) \left(\frac{e - \bar{q}}{v - \bar{b}} \right) - \gamma_{k,\phi} p_{\infty,k,\phi}. \tag{9}$$

This concludes the explicit thermodynamic closure for a multi-constituent mixture consisting of two condensable components and any number of non-condensable gases, with Eqs. (3), (4) and (6)-(9) providing all the necessary relations.

2.3. Simplified expression for $p = f(\rho, T)$

The expression of the pressure can be further simplified by neglecting the cubic term in Eq. (6), leading to the following explicit formula for p:

$$p_{approx} = \frac{a_1 + \sqrt{a_1^2 + 4a_0 a_2}}{2a_2} \tag{10}$$

This simplification leads to a relative error $\varepsilon = |p - p_{approx}|/p$ on the order of $\mathcal{O}\left(\frac{p}{p_\infty}\right)$ when only liquid is present ($\sum_{k=1}^{N} Y_{k,g} = 0$), or on the order of $\mathcal{O}\left(\frac{p^2}{p_\infty^2}\right)$ everywhere else ($\sum_{k=1}^{N} Y_{k,g} > 0$), corresponding to typical values of 5×10^{-4} or 2.5×10^{-7} in atmospheric conditions, respectively, for $p_\infty = 2 \times 10^8$ Pa.

This observation is corroborated by Fig. 2 (left) presenting, in barycentric coordinates in the domain of mole fractions for a complex mixture containing liquid ammonia NH_3, liquid water H_2O and gaseous nitrogen N_2, the relative error ε obtained with the quadratic formula (10): values below 10^{-7} are obtained almost everywhere, apart from the line corresponding to $\sum_{k=1}^{N} Y_{k,g} = 0$ where the error is nevertheless below 10^{-3}. The variation of ε with respect to gas components mass fraction $\sum_{k=1}^{N} Y_{k,g}$ (Fig. 2-right) confirms that the relative error is slightly larger than 10^{-4} in absence of gas components and about 10^{-7} when $\sum_{k=1}^{N} Y_{k,g}$ tends to 1.

3. Efficient phase transition solver

3.1. Motivation

Under certain thermodynamic conditions of pressure and temperature, phase transition can occur between liquid and gaseous phases. During this process, only the mass conservation equations of the involved components

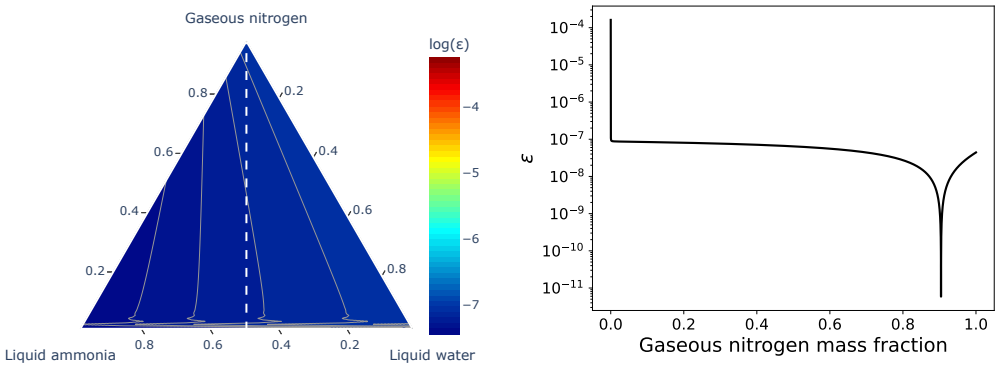

Figure 2: Relative error on the pressure ε with respect to the various constituents mass fractions of a mixture of liquid ammonia NH_3, liquid water H_2O and gaseous nitrogen N_2 in atmospheric condition (left) and with respect to gas components mass fraction following the white dashed line (right).

are modified by adding source terms. For a binary mixture, these source terms write:

$$\frac{\partial \rho Y_{1,l}}{\partial t} + \nabla \cdot \rho Y_{1,l}\mathbf{u} = \rho\nu_1 \left(g_{1,g} - g_{1,l}\right) \tag{11}$$

$$\frac{\partial \rho Y_{2,l}}{\partial t} + \nabla \cdot \rho Y_{2,l}\mathbf{u} = \rho\nu_2 \left(g_{2,g} - g_{2,l}\right) \tag{12}$$

$$\frac{\partial \rho Y_{1,g}}{\partial t} + \nabla \cdot \rho Y_{1,g}\mathbf{u} = -\rho\nu_1 \left(g_{1,g} - g_{1,l}\right) \tag{13}$$

$$\frac{\partial \rho Y_{2,g}}{\partial t} + \nabla \cdot \rho Y_{2,g}\mathbf{u} = -\rho\nu_2 \left(g_{2,g} - g_{2,l}\right) \tag{14}$$

where $g_{k,\phi}$ is the mass-specific partial Gibbs energy of component k at state ϕ and ν_k represents a relaxation parameter, for component k, controlling the rate at which thermodynamic equilibrium is reached. This last term depends in particular on the specific interfacial area, the temperature and the pressure. Although certain models exist [7–10, 12], its estimation is very complex as it can accurately be determined only when the interfacial area is known (for example for droplets and bubbly flows or for some stratified flows

[23]) or when mesh resolution is sufficiently high to capture interfaces at all spatial scales. A more practical and very common method [11, 14, 15, 24–26] is thus to consider that the relaxation parameter is infinitely large $\nu_k \to +\infty$ and so that the system is always at thermodynamic equilibrium. This hypothesis is valid for most of the flows of interest. However, it should be noted that it may be inadequate when the delay in evaporation and the appearance of metastable states are key features in the evolution of the flow.

Instead of using source terms, the equilibrium state is thus directly computed by solving a VLE at each time step from the state predicted by the hyperbolic transport of conservative variables. As the mixture specific volume $v = 1/\rho$, the internal energy e and the mass fractions of all the non-condensable gas components $Y_{k,g}$ for $k \geq 3$ remain constant during the phase transition, the goal of this VLE is to express the equilibrium state (p^*, T^*, $Y^*_{k,\phi}$ for $k = 1, 2$ and $\phi = l, g$) from these variables. Such work has already been presented in [11] for a single condensable species in equilibrium with a multi-component gas mixture. The present paper is devoted to the extension of this work to the case of two condensable components.

3.2. Expression of the thermodynamic equilibrium of a binary liquid-vapor mixture

The necessary condition for equilibrium in multi-phase mixtures is that the chemical potential of each condensable component ($k = 1, 2$) is the same in the two phases:

$$\mu_{k,l}(p, T, X_{k,l}) = \mu_{k,g}(p, T, X_{k,g}), \quad \text{for } k = 1, 2 \tag{15}$$

where $X_{k,\phi}$ is the mole fraction of component k in the phase ϕ, i.e.:

$$X_{k,\phi} = \frac{\frac{Y_{k,\phi}}{W_k}}{\sum_{k=1}^{N} \frac{Y_{k,\phi}}{W_k}}, \tag{16}$$

with W_k the molecular weight of component k. An equivalent condition is the equality of fugacities in both phases for each condensable component:

$$f_{k,l}(p, T, X_{k,l}) = f_{k,g}(p, T, X_{k,g}), \quad \text{for } k = 1, 2 \tag{17}$$

Adding a mass conservation constraint to the latter condition allows reformulating the VLE in the form of the so-called Rachford-Rice equation:

$$F(\tau_g) = \sum_{k=1}^{N} \frac{(K_k - 1)z_k}{1 + (K_k - 1)\tau_g} = 0, \tag{18}$$

where K_k is the equilibrium constant of the k^{th} component.

In the following, as mentioned above, it is further assumed that only two components are condensable ($k = 1$ and $k = 2$), which induces:

$$\forall k \geq 3, \quad K_k >> 1. \tag{19}$$

The Rachford-Rice equation then simplifies to:

$$F(\tau_g) = \frac{(K_1 - 1)z_1}{1 + (K_1 - 1)\tau_g} + \frac{(K_2 - 1)z_2}{1 + (K_2 - 1)\tau_g} + \sum_{k=3}^{N} \frac{z_k}{\tau_g} = 0, \tag{20}$$

where z_k is the total mole fraction of the k^{th} component e.g.:

$$\begin{cases} z_1 & = \overline{W} \dfrac{Y_{1,l} + Y_{1,g}}{W_1}, \\ z_2 & = \overline{W} \dfrac{Y_{2,l} + Y_{2,g}}{W_2}, \\ z_{k\geq 3} & = \overline{W} \dfrac{Y_{k\geq 3,g}}{W_{k\geq 3}}, \end{cases} \tag{21}$$

$\overline{W}$ being the mean molecular weight of the mixture:

$$\overline{W} = \left(\sum_{k=1}^{N} \frac{Y_{k,l} + Y_{k,g}}{W_k} \right)^{-1}, \tag{22}$$

and τ_g the mole fraction of the gas phase:

$$\tau_g = \sum_{k=1}^{N} \overline{W} \frac{Y_{k,g}}{W_k}. \tag{23}$$

The equilibrium constants of the condensable components, K_1 and K_2, are obtained from the fugacity constraint (Eq. (17)). Under the assumptions of the NASG EoS, the vapor phase constituents behave like a perfect gas. The fugacity of the vapor components thus reduces to:

$$f_{1,g} = X_{1,g}\, p \tag{24}$$

$$f_{2,g} = X_{2,g}\, p \tag{25}$$

The fugacity of the liquid components is proportional to the pure component vapor pressure $p_{sat,k}$:

$$f_{1,l} = X_{1,l}\, p_{sat,1}(T)\, a_1(T, X_{1,l})\, \mathcal{P}_1(p, T) \tag{26}$$

$$f_{2,l} = X_{2,l}\, p_{sat,2}(T)\, a_2(T, X_{2,l})\, \mathcal{P}_2(p, T) \tag{27}$$

where a_k $(k = 1, 2)$ refers to the so-called activity coefficient of the k^{th} constituent, which allows taking into account non-ideal solutions, and $\mathcal{P}_k$ is its Poynting factor:

$$\mathcal{P}_k(p, T) = exp\left(\frac{\int_{p_{sat,k}}^{p} v_{k,l}^{m}(p, T) dp}{RT} \right) \tag{28}$$

where R is the universal gas constant and $v_{k,l}^{m}$ corresponds to the molar specific volume at liquid state of the k^{th} component.

As this factor accounts for the effect of liquid compression on fugacity, it can be often neglected (namely $\forall k = 1, 2,\ \mathcal{P}_k(p, T) = 1$) as long as the pressure remains low or moderate.

By definition, the equilibrium constant of the condensable components corresponds to the ratio between its vapor and its liquid mole fractions:

$$K_1 = \frac{X_{1,g}}{X_{1,l}} \tag{29}$$

$$K_2 = \frac{X_{2,g}}{X_{2,l}} \tag{30}$$

Therefore, by combining Eqs. (24), (26) and (29) and, Eqs. (25), (27) and (30), the equilibrium constants of the condensable components write:

$$K_1 = \frac{p_{sat,1}(T)\, a_1(T, X_{1,l})\, \mathcal{P}_1(p, T)}{p} \tag{31}$$

$$K_2 = \frac{p_{sat,2}(T)\, a_2(T, X_{2,l})\, \mathcal{P}_2(p, T)}{p} \tag{32}$$

3.3. Vapor-liquid equilibrium of a NH_3-H_2O mixture

Considering a mixture of ammonia NH_3 and water H_2O, where NH_3 is identified by the index 1 and H_2O by the index 2, the activity coefficient of each condensable component of the mixture is computed with the NRTL model [5]:

$$\ln\left(a_1(T, X_{1,l})\right) = (1 - X_{1,l})^2 \left[\tau_{21} \left(\frac{G_{21}}{X_{1,l} + (1 - X_{1,l})G_{21}}\right)^2 + \frac{\tau_{12} G_{12}}{((1 - X_{1,l}) + X_{1,l} G_{12})^2}\right] \tag{33}$$

$$\ln\left(a_2(T, X_{2,l})\right) = (1 - X_{2,l})^2 \left[\tau_{12} \left(\frac{G_{12}}{X_{2,l} + (1 - X_{2,l})G_{12}}\right)^2 + \frac{\tau_{21} G_{21}}{((1 - X_{2,l}) + X_{2,l} G_{21})^2}\right] \tag{34}$$

where,

$$\tau_{12} = a_{12} + \frac{b_{12}}{T} \tag{35}$$

$$\tau_{21} = a_{21} + \frac{b_{21}}{T} \tag{36}$$

and,

$$G_{12} = \exp\left(-\alpha_{12}\tau_{12}\right) \tag{37}$$

$$G_{21} = \exp\left(-\alpha_{12}\tau_{21}\right) \tag{38}$$

G_{ij} is an energy parameter characteristic of the interaction between species i and j and α_{12} corresponds to the non-randomness of the mixture. The parameters $a_{12}, b_{12}, a_{21}, b_{21}$ and α_{12} were fitted to a set of vapor-liquid equilibrium data [27–30] resulting in a mean deviation $|p_{exp} - p_{calc}|/p_{exp}$ equal to 5.6%. The fitted values are given in Tab. 1.

System	$NH_3 + H_2O$
a_{12}	1.4223
b_{12}	-739.67
a_{21}	-1.7681
b_{21}	406.87
α_{12}	0.2

Table 1: Fitted parameters of the NRTL model for ammonia and water activity coefficients in the $(NH_3 + H_2O)$ mixture.

The vapor pressures of pure components are calculated using the Antoine equation:

$$\log_{10}(p_{sat,i}(T)) = A_i - \frac{B_i}{C_i + T} \tag{39}$$

with $p_{sat,i}$ in bar.

For water, the parameters A_i, B_i and C_i were fitted to experimental data in the temperature range 273K $\leq T \leq$ 613K [31–33] whereas for ammonia, due to a lack of data, the values given by the NIST were used (see Tab. 2).

Component	H_2O	NH_3
A_i	5.139118	4.86886
B_i	1702.018315	1113.928
C_i	-41.719448	-10.409

Table 2: Parameters of the Antoine equation for the vapor pressure of pure components.

The VLE curves obtained by solving the Rachford-Rice equation with the above modeling of activity coefficient are compared with the experimental data of Rizvi et al. [27] for three temperatures in Fig. 3. Globally, the bubble and dew point pressures of the mixture are accurately calculated with the proposed model for all the range of NH_3 mole fraction. It must be underlined that these results were obtained by neglecting the Poynting factor.

3.4. Simplified problem: VLE at given $(p, T, Y_{k\geq 3,g})$

To illustrate the problem to be solved, and to provide an initial condition for the simulations, the case is considered where equilibrium values for pressure, temperature and non-condensable component mass fractions are imposed in the VLE calculation (i.e. $p = p^*$, $T = T^*$ and $Y_{k,g} = Y^*_{k,g}$ for $k \geq 3$). In these conditions, the condensable component mass fractions $Y^*_{k,\phi}$ for $k = 1, 2$ and $\phi = l, g$ are the only unknowns of the VLE problem, since the mixture specific volume v^* and mixture internal energy e^* at equilibrium are directly computed with the EoS from p^*, T^* and $Y^*_{k,\phi}$ for $k = 1, ..., N$ and $\phi = l, g$. Figure 4 depicts the situation.

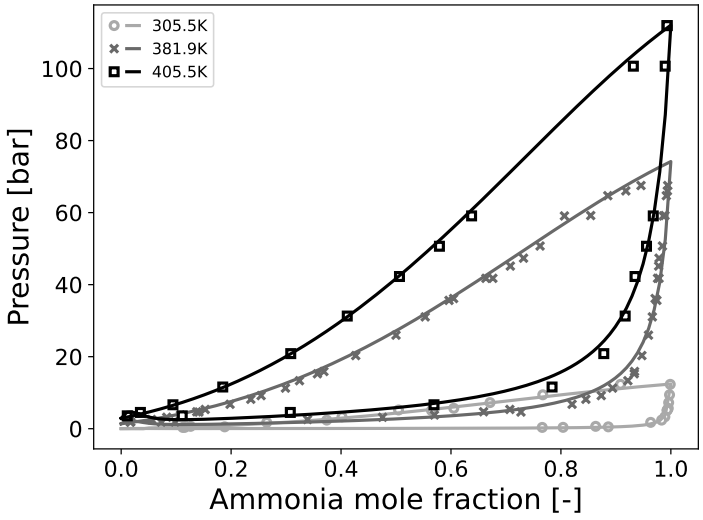

Figure 3: Comparison of vapor-liquid equilibria obtained by solving the Rachford-Rice equation with a NRTL model for activity coefficients with experimental data of [27] in symbols. Dew and bubble point pressure curves are plotted as function of the ammonia mole fraction for a binary multi-phase mixture of NH_3 and H_2O at temperature $T = 305.5$K, $T = 381.9$K and $T = 405.5$K.

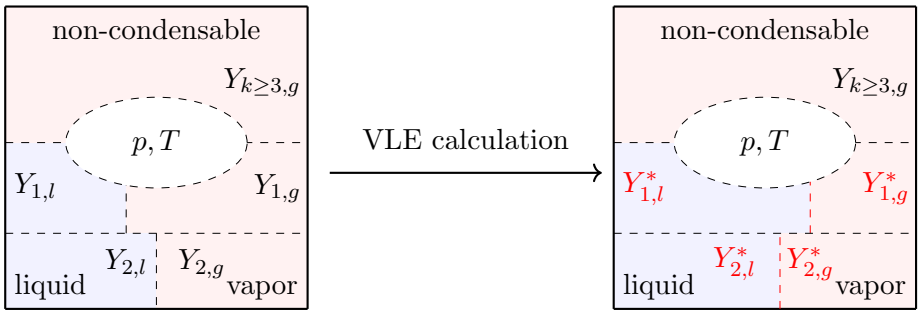

Figure 4: Representation of a control volume in the flow model for the simplified problem, at constant $(p, T, Y_{k\geq 3,g})$. The properties identified with the superscript * are modified by the VLE calculation.

Under these conditions, the simplified Rachford-Rice Eq. (20) reduces to the following quadratic equation for τ_g:

$$a_2\tau_g^2 - a_1\tau_g - a_0 = 0, \tag{40}$$

with

$$\begin{cases} a_2 = (K_1 - 1)(1 - K_2), \\ a_1 = (K_1 - 1)z_1 + (K_2 - 1)z_2 + \sum_{k\geq 3}^{N} z_k[(K_1 - 1) + (K_2 - 1)], \\ a_0 = \sum_{k\geq 3}^{N} z_k. \end{cases} \tag{41}$$

yielding an explicit analytical solution for τ_g:

$$\tau_g(p, T, Y_{k\geq 3,g}) = \frac{a_1 + \sqrt{a_1^2 + 4a_0a_2}}{2a_2}. \tag{42}$$

Note that, since z_k remains constant through phase transition $\forall k$, knowledge of τ_g fully defines the liquid and gas mass fraction of each component as:

$$\begin{cases} Y_{k,l} &= y_k \dfrac{1 - \tau_g}{1 + (K_k - 1)\tau_g}, \\ Y_{k,g} &= y_k \dfrac{K_k\tau_g}{1 + (K_k - 1)\tau_g}, \end{cases} \tag{43}$$

trivially conserving the mass fraction y_k of each condensable component :

$$y_k = z_k \frac{W_k}{\overline{W}}. \tag{44}$$

Figure 5 (left) shows the classical behavior of a binary NH_3-H_2O mixture, e.g. with $z_{k\geq 3} = X_{k\geq 3,g} = 0$, at a pressure $p = 2$ bar. The bubble and dew point temperatures, obtained by solving the simplified Rachford-Rice Eq. (20) respectively with $\tau_g = 0$ and $\tau_g = 1$ (see Appendix B), are plotted in function of NH_3 mole fraction z_1. As expected, the two curves cross at the

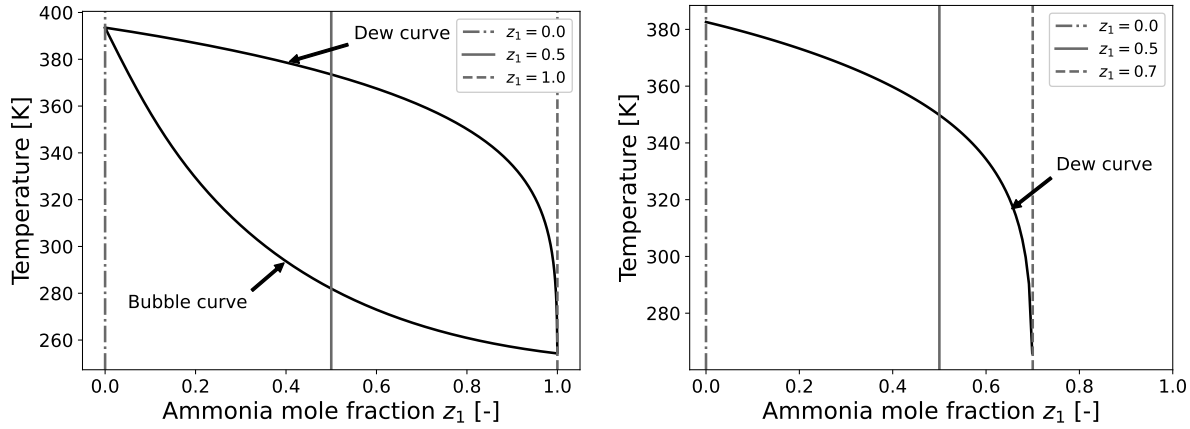

Figure 5: Vapor-liquid equilibria at pressure $p = 2$ bar: dew and bubble temperature curves as a function of the NH_3 mole fraction z_1 for a binary multi-phase mixture of NH_3 and H_2O at left and, for a complex mixture with two condensable components NH_3 and H_2O and non-condensable gases ($\sum_{k\geq 3}^{N} z_k = \sum_{k\geq 3}^{N} X_{k,g} = 0.3$) at right.

saturation temperature of NH_3 at $z_1 = 1$ ($T_{sat,1} = 254$ K), and of H_2O at $z_1 = 0$ ($T_{sat,2} = 393$ K). The right plot of Fig. 5 repeats the left one when adding a non-condensable gas mole fraction of $z_{k\geq 3} = X_{k\geq 3,g} = 0.3$. As previously noted by Chiapolino et al. [11] in the case of one condensable component, the bubble point disappears: for every amount of non-condensable gas, no matter how small, one can find a solution to the VLE problem using Eq. (42) including small quantities of gases.

Figure 6 shows the equilibrium gas phase mole fraction τ_g for three NH_3 contents $z_1 = (0, 0.5, 1 - \sum_{k\geq 3}^{N} z_k)$ (materialized by vertical lines in Fig. 5) as a function of temperature at $p = 2$ bar for a binary $NH_3 - H_2O$ mixture (left) and for a complex mixture with two condensable components NH_3 and H_2O and with a mole fraction of non-condensable gas $\sum_{k\geq 3}^{N} z_k = \sum_{k\geq 3}^{N} X_{k,g} = 0.3$ (right). Sharp jumps are obtained for pure components $z_1 = (0, 1)$ and a smooth transition is observed for the binary mixture ($z_1 = 0.5$) between

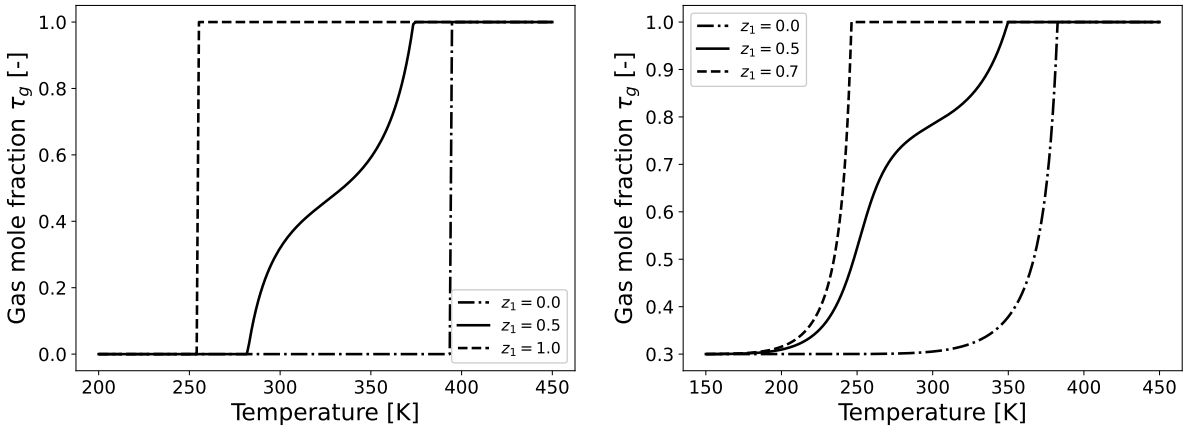

Figure 6: Equilibrium gas phase mole fraction τ_g for three NH_3 contents $z_1 = (0, 0.5, 1 - \sum_{k\geq 3}^{N} z_k)$ (materialized by vertical lines in Fig. 5) as a function of temperature at pressure $p = 2$ bar. At left, the mixture is binary $NH_3 - H_2O$ ($\sum_{k\geq 3}^{N} z_k = 0.0$). At right, the mixture contains two condensable components NH_3 and H_2O and a mole fraction of non-condensable gas $\sum_{k\geq 3}^{N} z_k = 0.3$.

bubble and dew points. However, in presence of a non-condensable gas, smooth change is always obtained until dew point whatever the value of the ammonia content z_1. A discontinuity in the solution of the VLE problem is thus observed near the dew point for all the mixtures and, also near the bubble point for binary mixtures. In these regions, the Rachford-Rice equation is not valid and a special treatment has to be provided. Therefore, at and above the dew temperature, the mixture is fully gaseous and the gas mole fraction τ_g is set to one. And, for binary mixtures only, the condensable components are in liquid state at and below the bubble temperature: the gas mole fraction τ_g is thus set to zero. The case of pure component mixtures ($z_1 = (0, 1)$ in Fig. 6) is directly covered by previous checks as bubble and dew points curves cross at pure component saturation temperature.

The solution of the VLE problem at given $(p, T, Y_{k\geq 3,g})$ is given by the

algorithm 1. Note that, since temperature and pressure are related at saturation, the reasoning can also be applied to pressure by reversing the sign of the comparisons.

if $Y_{k\geq 3,g} = 1$ **then**
  Only non-condensable gas is present: No need to compute equilibrium;
else
  Compute dew temperature (or equivalently pressure).
  if $T > T_{dew}$ *(or equivalently* $p < p_{dew}$*)* **then**
    Full vapor mixture
    $\tau_g \leftarrow 1$
  else
    if $Y_{k\geq 3,g} = 0$ **then**
      The mixture is a binary mixture.
      Compute bubble temperature (or equivalently pressure).
      if $T < T_{bubble}$ *(or equivalently* $p > p_{bubble}$*)* **then**
        Full liquid mixture
        $\tau_g \leftarrow 0$
      else
        Solve Rachford-Rice equation.
        $\tau_g \leftarrow \tau_g(p, T, Y_{k\geq 3,g})$ (Eq. (42))
      end
    else
      Solve Rachford-Rice equation.
      $\tau_g \leftarrow \tau_g(p, T, Y_{k\geq 3,g})$ (Eq. (42))
    end
  end
  Compute liquid and gas mass fractions of each condensable components using Eq. (43).
end

Algorithm 1: VLE calculation procedure at constant pressure $p = p^*$, temperature $T = T^*$ and non-condensable gas component mass fractions $Y_{k,g} = Y^*_{k,g}$ for $k \geq 3$.

3.5. VLE at given $(\rho, e, Y_{k\geq 3,g})$

In simulations of multiphase flows, the conservative variables (mass, momentum and total energy) are usually transported, so that thermo-chemical

equilibrium can no longer be achieved considering constant (p, T) as in Sec. 3.4. Indeed, as depicted in Fig. 7, density $\rho = \rho^*$ and internal energy $e = e^*$ are now invariant through phase change while the pressure p^* and temperature T^* at equilibrium become unknown in addition to the condensable component mass fractions $Y^*_{k,\phi}$ for $k = 1, 2$ and $\phi = l, g$. As previously noticed in

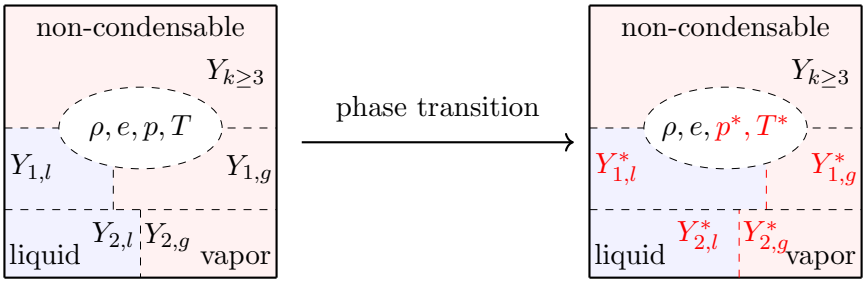

Figure 7: Representation of a control volume in the flow model during the phase transition step. The properties identified with the superscript * are modified through the relaxation process.

Sec. 3.4, the knowledge of the gas mole fraction τ_g^* at equilibrium is sufficient to determine the mixture composition. Hence, the problem to be solved involves three unknowns (p^*,T^*,τ_g^*). Conservation of mass $\rho = \rho^*$ and internal energy $e = e^*$ provides the two first relations while the simplified Rachford-Rice Eq. (20) gives the last. The problem to be solved is thus summarized by the following system:

$$\begin{cases} v = v^* = \sum_{k=1,2} \left[Y^*_{k,l} v_{k,l}(T^*, p^*) + Y^*_{k,g} v_{k,g}(T^*, p^*) \right] + \sum_{k=3}^{N} Y_{k,g} v_{k,g}(T^*, p^*) \\ e = e^* = \sum_{k=1,2} \left[Y^*_{k,l} e_{k,l}(T^*, p^*) + Y^*_{k,g} e_{k,g}(T^*, p^*) \right] + \sum_{k=3}^{N} Y_{k,g} e_{k,g}(T^*, p^*) \\ \frac{(K_1-1)z_1}{1+(K_1-1)\tau_g^*} + \frac{(K_2-1)z_2}{1+(K_2-1)\tau_g^*} + \sum_{k\geq 3}^{N} \frac{z_k}{\tau_g^*} = 0 \end{cases} \tag{45}$$

where $v = \frac{1}{\rho}$ represents the specific volume of the mixture. Such problem does not have an explicit solution, and efficient strategies have to be developed.

Figure 8 shows the surfaces typically formed by the τ_g, p and T values that are solutions to each of the three equations in the system (45). The VLE solution is obtained at the intersection of the three surfaces. It can be remarked that this intersection is always unique due to the convex nature of the NASG EoS. This unicity is very important, as it is a prerequisite for the use of the VLE computation strategy which is discussed next.

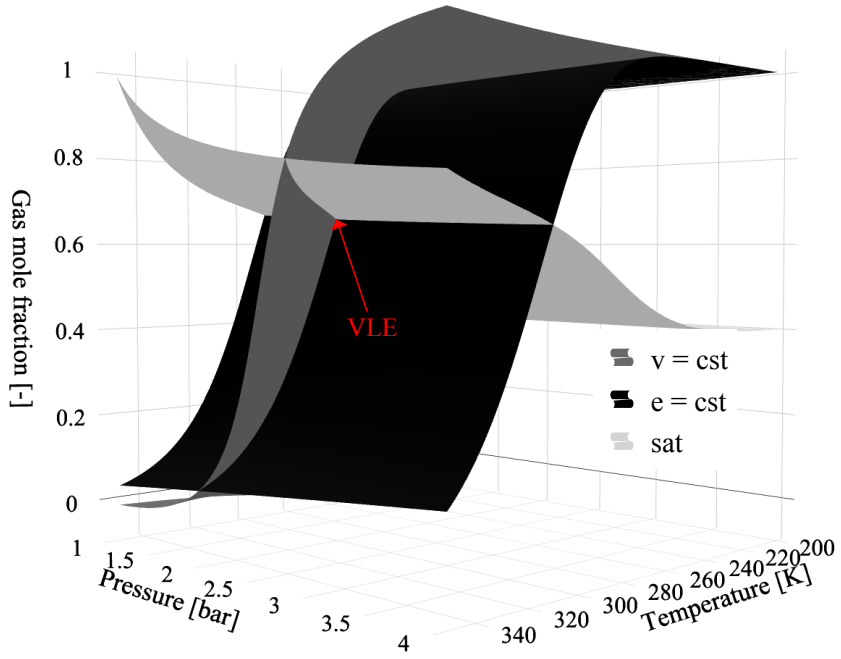

Figure 8: Surface solution of the three equations in the system (45). The reference state corresponds to the VLE at $P = 2$ bar and $T = 300$ K with a mole fraction of non-condensable gas ($\sum_{k\geq 3}^{N} z_k = \sum_{k\geq 3}^{N} X_{k,g} = 0.4$) computed with the algorithm of Sec. 3.4.

In order to save computational time, the presence of condensable component is first checked and, the thermodynamic equilibrium is not calculated if only non-condensable gas is present. As the VLE solution is unique, a proof by contradiction can then be applied to treat the limit case where only vapor is present. The pressure p_{test} and temperature T_{test} are thus computed by

assuming that $\tau_g = 1$. The pressure p_{test} is then compared to the dew point pressure p_{dew} calculated from Eq. (B.4). If the pressure has a physical value ($p_{test} > 0$) and is below the dew point ($p_{test} < p_{dew}$), the set ($\tau_g = 1$, p_{test}, T_{test}) is a solution of the VLE problem. As this problem admits a unique solution, the equilibrium gas mole fraction is $\tau_g^* = 1$ and, the equilibrium pressure p^* and temperature T^* are $p^* = p_{test}$ and $T^* = T_{test}$. In absence of non-condensable components, the limit case of a full liquid mixture has also to be checked. The same type of reasoning as for dew point is used: the pressure p_{test} and temperature T_{test} are computed by assuming that $\tau_g = 0$. The pressure p_{test} is then compared to the bubble point pressure p_{bubble} determined using Eq. (B.2): If p_{test} is above the bubble point pressure ($p_{test} > p_{bubble}$), the set ($\tau_g = 0$, p_{test}, T_{test}) is the solution of the VLE problem: $\tau_g^* = 0$, $p^* = p_{test}$ and $T^* = T_{test}$. Finally, if the solution doesn't match any of the limit cases, the mixture at equilibrium is in a two-phase state ($0 < \tau_g < 1$). A classical Newton-Raphson's algorithm is then used to determine the solution (τ_g^*, p^*, T^*) of the VLE problem. Details of the resolution are given in Appendix C.

The overall methodology for solving the VLE problem at given $(\rho, e, Y_{k\geq 3,g})$ is summarized in the algorithm 2.

if $Y_{k\geq 3} = 1$ **then**
  Only non-condensable gas is present: No need to compute equilibrium
else
  Search for a solution without liquid
  → Compute pressure p_{test} and temperature T_{test} with the EoS assuming a full vapor mixture.
  → Compute dew point pressure p_{dew}.
  if $0 < p_{test} < p_{dew}$ **then**
    Full vapor mixture
    $\tau_g^* \leftarrow 1$, $p^* \leftarrow p_{test}$ and $T^* \leftarrow T_{test}$
  else
    if $Y_{k\geq 3,g} = 0$ **then**
      The mixture is a binary mixture
      Search for a solution without vapor
      → Compute pressure p_{test} and temperature T_{test} with the EoS assuming a full liquid mixture.
      → Compute bubble point pressure p_{bubble}.
      if $p_{test} > p_{bubble}$ **then**
        Full liquid mixture
        $\tau_g^* \leftarrow 0$, $p^* \leftarrow p_{test}$ and $T^* \leftarrow T_{test}$
      else
        Search for a solution with vapor and liquid
        → Solve the system using a Newton-Raphson algorithm: $(\tau_g^{NR}, p^{NR}, T^{NR})$.
        $\tau_g^* \leftarrow \tau_g^{NR}$, $p^* \leftarrow p^{NR}$ and $T^* \leftarrow T^{NR}$
      end
    else
      Search for a solution with vapor and liquid
      → Solve the system using a Newton-Raphson algorithm: $(\tau_g^{NR}, p^{NR}, T^{NR})$.
      $\tau_g^* \leftarrow \tau_g^{NR}$, $p^* \leftarrow p^{NR}$ and $T^* \leftarrow T^{NR}$
    end
  end
  Compute liquid and gas mass fractions of each condensable component using Eq. (43).
end

Algorithm 2: VLE calculation procedure at constant density $\rho = \rho^*$, internal energy $e = e^*$ and non-condensable gas component mass fractions $Y_{k,g} = Y_{k,g}^*$ for $k \geq 3$.

4. 1D numerical results

The behavior and robustness of the present modelling strategy are tested on series of 1D shock tube cases. The shock tube has already been used by Chiapolino et al. [11] to validate their approximated VLE algorithm as the presence of shock waves, contact discontinuities and rarefaction fans create arduous flow conditions. In all test cases, the tube is 1 m long and the initial discontinuity is located at 0.5 m. The mixture is made of ammonia NH_3, water H_2O and air. For sake of simplicity, air is modeled by nitrogen N_2. This approximation is perfectly valid since nitrogen represents about 78% of air composition. The thermodynamic parameters for NH_3, H_2O and N_2 are given in Appendix A. The boundary conditions are non-reflecting outlet boundary condition (NSCBC) initially proposed by [34] and recently extended to NASG EoS by [18]. The flow is solved using a three-step Runge-Kutta numerical scheme combined with a Godunov spatial integration where fluxes are computed using a HLLC Riemann solver. The whole method is implemented within the YALES2 solver [35] for unstructured grids. Originally developed to solve Low-Mach number flows, an explicit compressible solver has recently been developed to solve all-Mach number flows. The 1D domain is composed of 1000 equidistant nodes.

4.1. Effect of the simplified pressure formulation

The validity of the simplified expression for pressure (Eq. (10)) is discussed through two shock tube cases. In both cases, the domain is filled with a two-phase mixture made of condensable NH_3 and H_2O and non-condensable N_2 at temperature $T_l = T_r = 300$ K, where the subscripts r and l refer to right and left sides, respectively. The mole fraction of each components in

the mixture is $z_l = z_r = [z_{\mathrm{NH_3}}\ z_{\mathrm{H_2O}}\ z_{\mathrm{N_2}}] = [0.2\ 0.2\ 0.6]$. The velocity is set to $u_l = u_r = 0$ m.s^{-1} and the pressure in the right side is $p_r = 1$ bar. The pressure in the left side is $p_l = 2$ bar in the first case and $p_l = 50$ bar in the second case. Figure 9 shows the pressure field at time $t = 1$ ms for the first simulation and, $t = 0.5$ ms for the second one.

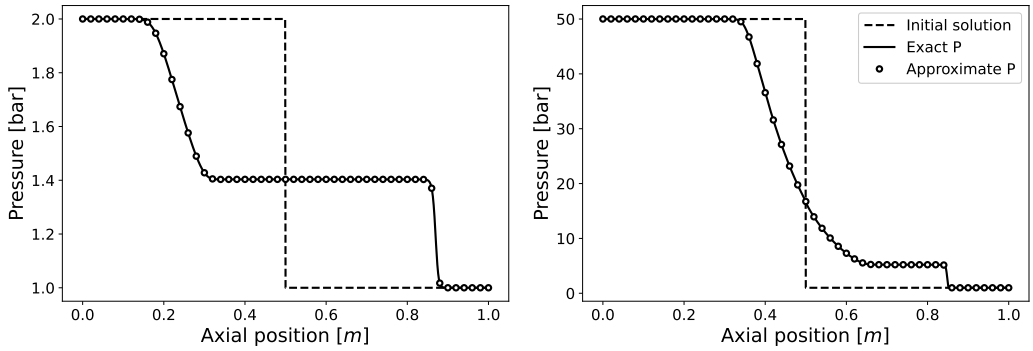

Figure 9: Comparison between the exact pressure (thick lines) and the approximate one (symbols). Shock tube test with a two-phase mixture made of liquid NH_3, liquid water, vapor NH_3, vapor water and air. The dashed lines represent the initial conditions: $p_l = 2.10^5\ Pa$, $p_r = 1.10^5 Pa$ (left), $p_l = 50.10^5\ Pa$, $p_r = 1.10^5 Pa$ (right) and $T_l = T_r = 300\ K$, $u_l = u_r = 0 m.s^{-1}$, $z_{left} = z_{right} = [0.2\ 0.2\ 0.6]$. Final time: $t = 1ms$ (left) and $t = 0.5ms$ (right). Mesh: 1000 cells. For the sake of clarity, only 50 symbols out of 1000 are plotted for the approximate solution.

Perfect agreement is obtained between the exact formulation (Eq. (6)) and the simplified expression (Eq. (10)). The L_2 norms of the relative error ϵ on pressure caused by the simplified formulation are $\epsilon = 3.33.10^{-7}$ ($p_l = 2$ bar) and, $\epsilon = 2.08.10^{-4}$ ($p_l = 50$ bar). As expected from discussion in Sec. 2.3, the error increases with pressure, but remains very small. The use of the simplified expression is particularly interesting for its associated calculation cost as the pressure computation is significantly cheaper than with the iterative resolution of the exact expression. In both cases, the simulation

cost per CPU and per node is thus reduced by around 41%, including 64% for the VLE calculation. Because of its low cost and very good accuracy, the simplified expression (Eq. (10)) is used in all subsequent simulations.

4.2. Robustness of the VLE algorithm

Three shock tube cases inspired by [11] are now simulated to demonstrate the robustness and behavior of the VLE algorithm among several characteristic mixture conditions: (1) far from the phase bounds, (2) with non-condensable air in major proportion and (3) with condensable components at liquid state in major proportion.

4.2.1. Shock tube test with a mixture far from the phase bounds

A two-phase mixture with initial mole fraction set to $z_l = z_r = [z_{\mathrm{NH_3}}\ z_{\mathrm{H_2O}}\ z_{\mathrm{N_2}}] = [0.2\ 0.2\ 0.6]$ is considered throughout the entire domain. The temperature and velocity are uniform and equal to $T_l = T_r = 300$ K and $u_l = u_r = 0$ m.s^{-1}. The initial pressure is set to $p_l = 2$ bar on the left and $p_r = 1$ bar on the right. The results are shown at time $t = 1$ ms in Fig. 10.

In this case, the shock compression and the resulting rise in temperature cause the condensables to evaporate. While the rarefaction wave upstream of the shock causes a temperature drop and condensation of NH_3 and H_2O. These results are physically consistent and in accordance with those obtained by [11] for a monospecies liquid.

4.2.2. Shock tube test with a mixture with non-condensable air in major proportion

The entire domain is filled with an air mole fraction $z_{\mathrm{N_2}} = 0.98$. The small remaining molar fraction is divided equally between the two condensables. The initial pressure is set to $p_l = 6$ bar on the left and $p_r = 2$ bar on the

right. The temperature is $T_l = T_r = 280$ K and the velocity is $u_l = u_r = 0$ m.s^{-1}. Figure 11 shows the results obtained at $t = 1$ ms.

As in the previous case, evaporation and condensation caused by the shock compression and the rarefaction wave respectively are observed. However, due to the small amount of condensable, the liquid ammonia and water evaporates completely in the compression zone and all the vapor water condenses in the expansion zone. This illustrates the ability of the method to correctly handle the full transition of a species from one phase to another without oscillation.

4.2.3. Shock tube test with a mixture with condensable components at liquid state in major proportion

The last shock-tube test concerns the case where the non-condensable air is in negligible proportion $z_{N_2} = 10^{-5}$ and the condensable components form a mixture of $z_{NH_3} = 0.2$ and $z_{H_2O} = 0.7 - 10^{-5}$ in the liquid state. This mixture composition is uniform throughout the tube. The temperature and velocity are also uniform, at $T_l = T_r = 280$ K and $u_l = u_r = 0$ m.s^{-1}. The pressure is $p_l = 4$ bar on the left and $p_r = 2$ bar on the right. The flow conditions after $t = 0.5$ ms is shown in Fig. 12.

The results are also in line with [11]: as the heat capacity of the liquid is higher than that of the gas, a slight evaporation is observed, but the case is quasi-isothermal. It is interesting to note that the appearance of vapor in the liquid mixture has an effect on the density that changes the velocity and temperature. Despite its density modification, the appearance of vapor in the liquid is simulated without oscillation, demonstrating the stability of the method.

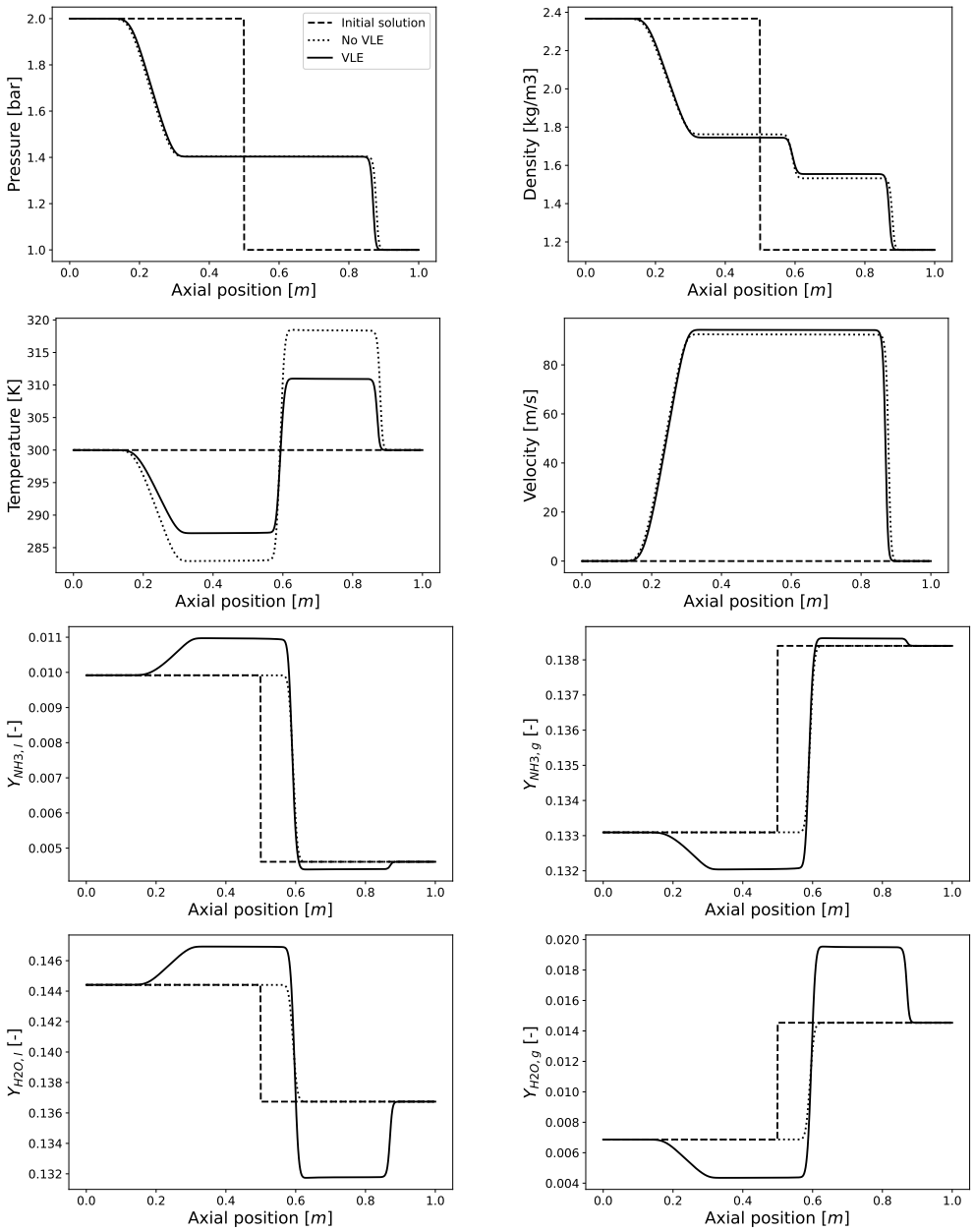

Figure 10: Shock tube test with a two-phase mixture made of liquid NH_3, liquid water, vapor NH_3, vapor water and air. The solid and dotted lines represent the solutions at the last time step with and without phase transition, respectively. The dashed lines represent the initial conditions: $p_l = 2.10^5\ Pa$, $p_r = 1.10^5 Pa$, $T_l = T_r = 300\ K$, $u_l = u_r = 0m.s^{-1}$, $z_l = z_r = [0.2\ 0.2\ 0.6]$. Final time: $t = 1ms$. Mesh: 1000 cells.

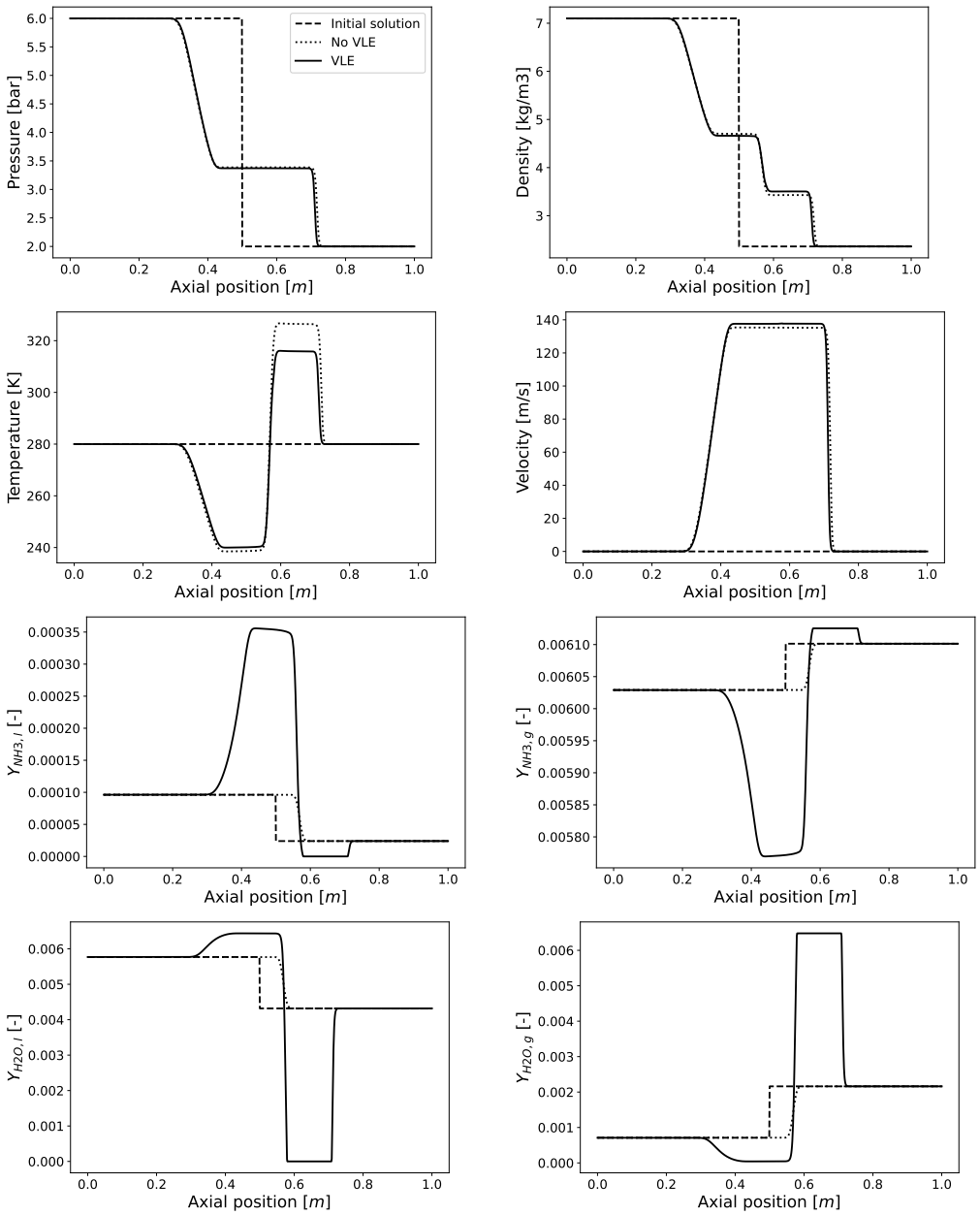

Figure 11: Shock tube test with a two-phase mixture made of liquid NH_3, liquid water, vapor NH_3, vapor water and air. The solid and dotted lines represent the solutions at the last time step with and without phase transition, respectively. The dashed lines represent the initial conditions: $p_l = 6.10^5\ Pa$, $p_r = 2.10^5 Pa$, $T_l = T_r = 280\ K$, $u_l = u_r = 0 m.s^{-1}$, $z_l = z_r = [10^{-2}\ 10^{-2}\ 0.98]$. Final time: $t = 1ms$. Mesh: 1000 cells.

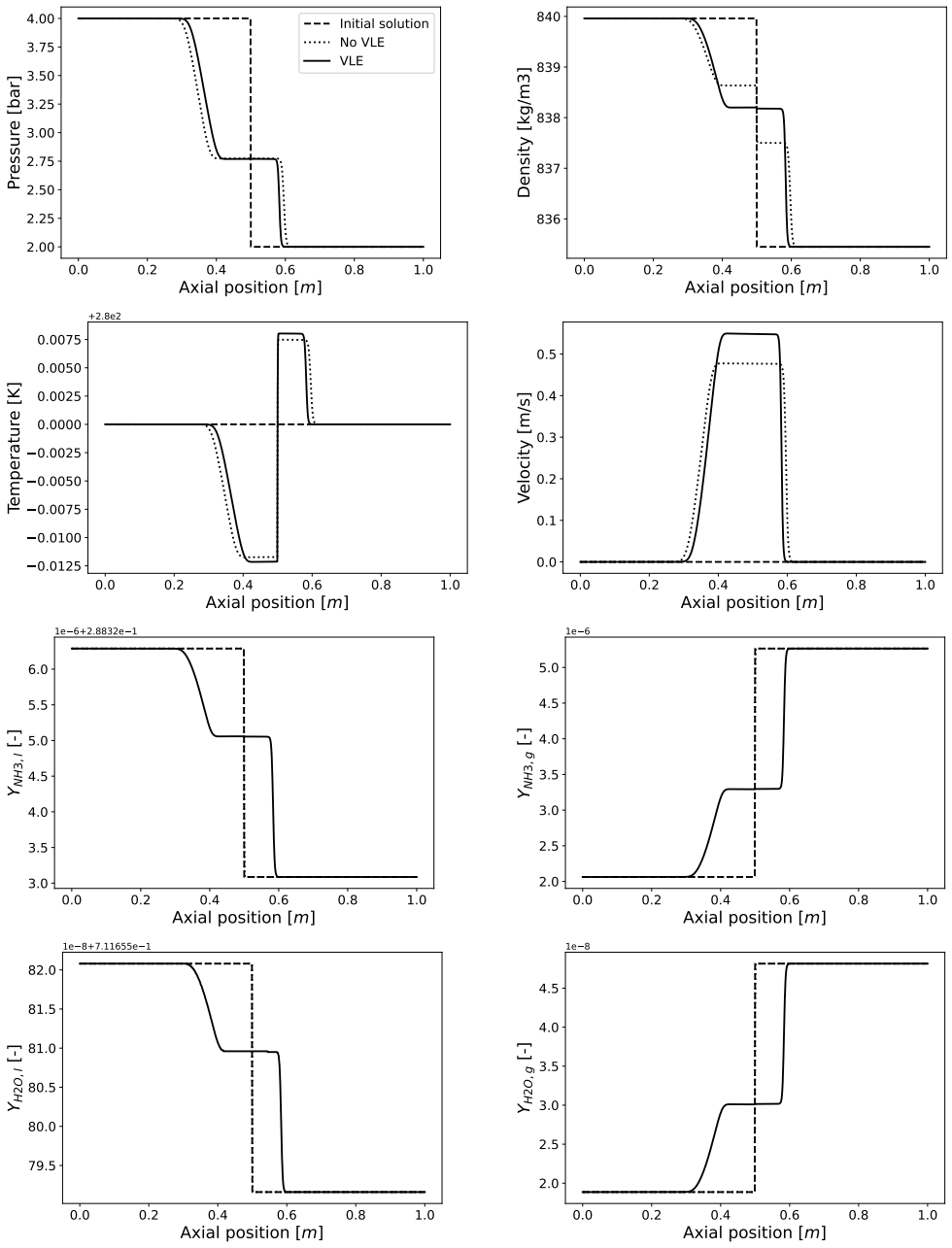

Figure 12: Shock tube test with a two-phase mixture made of liquid NH_3, liquid water, vapor NH_3, vapor water and air. The solid and dotted lines represent the solutions at the last time step with and without phase transition, respectively. The dashed lines represent the initial conditions: $p_l = 4.10^5\ Pa$, $p_r = 2.10^5 Pa$, $T_l = T_r = 280\ K$, $u_l = u_r = 0 m.s^{-1}$, $z_l = z_r = [0.3\ 0.7 - 10^{-5}\ 10^{-5}]$. Final time: $t = 0.5$ ms. Mesh: 1000 cells.

5. 2D simulation of a two-phase jet from a leaking tank

The capabilities of the present method is now illustrated on phase-change two-phase jet. The chosen case represents a typical configuration of a leak in a pressurised liquefied gas tank. This type of accident is particularly challenging to simulate because it involves many violent physical phenomena. The pressure drop caused by the leak creates a flash evaporation of the liquid. The resulting expansion then creates an acceleration that can lead to the formation of shocks at the outlet of the release. A very cold two-phase spray is then produced downstream of the leak. When it comes into contact with the surrounding humid air, the water in the air condenses, creating a two-phase mixture containing vapor and liquid water, gas from the reservoir in liquid and evaporated form, and non-condensable air.

5.1. Configuration and numerical set up

A 2D configuration of a leak from a tank containing pressurized liquid ammonia is considered. As shown in Fig. 13, it consists of a tank, a channel from which liquefied gas is leaking and a large domain representing the atmosphere. The ammonia is stored at 4.1 bar and $T = 271$ K (1 K below the saturation temperature of ammonia). The ambiant is composed of non-condensable air, represented by nitrogen N_2, and vapor water H_2O at $P = 1$ bar and $T = 283$ K. The thermodynamic parameters are provided in Appendix A. The relative air humidity is set to 80%, corresponding to autumn morning conditions. The specific humidity, i.e. the vapor mass fraction in the ambiant, is thus $Y_{H_2O,g} = 6.1285 \times 10^{-3}$.

The inlet and outlet boundary conditions are NSCBC boundary condition [34] extended to NASG EoS [18]. A subsonic inlet condition is imposed

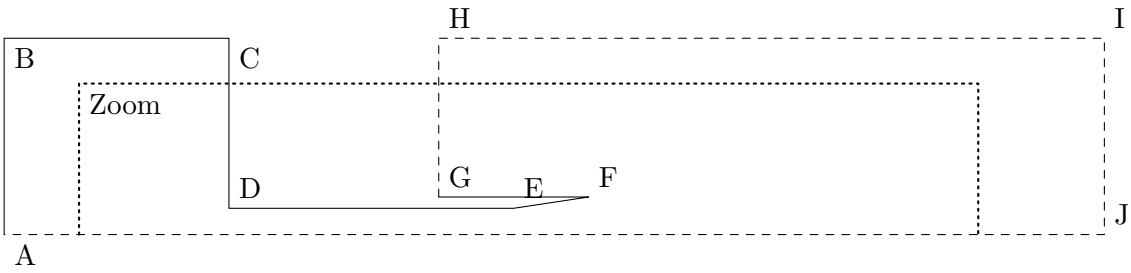

	X (abscissa) (mm)	Y (mm)		X(abscissa) (mm)	Y (mm)
A	-80	0	F	-2	2.5
B	-80	52	G	-22	2.5
C	-50	52	H	-22	52
D	-50	1.75	I	200.5	52
E	-12	1.75	J	200.5	0

Figure 13: Geometrical data for half the computational domain of the 2D liquid ammonia leakage case.

along the segment BC in order to maintain the static pressure $P = 4.1$ bar, the temperature $T = 271$ K and composition $Y_{\mathrm{NH_3},l} = 1.0$ in the upper part of the tank. A subsonic outlet is placed along the segment IJ, imposing $P = 1$ bar. The remaining segments are treated as slip wall boundary conditions.

As for the 1D cases, the flow is solved with a three-step Runge-Kutta numerical scheme for time integration and a Godunov scheme for spatial integration. In order to reduce the numerical error, the spatial scheme accuracy is increased up to the second order using a MUSCL reconstruction for unstructured grid with a Sweby limiter ($\beta = 1.8$). The gradients involved in the MUSCL reconstruction are computed using the linear finite-element projection from [36]. A SLAU2 [Simple Low-dissipation AUSM (Advection Upstream Splitting Method)] Riemann solver is also used instead of the HLLC. Originally proposed by [37] and later improved in its second version by [38],

SLAU2 is a low-dissipative Riemann solver, especially at low Mach numbers, which allows small-scale spray destabilisation to be captured.

The domain is initially discretized with 220 000 triangles with a characteristic size between $\Delta x_{init} = 0.5$ mm and $\Delta x_{init} = 0.7$ mm. To ensure a good description of the spray, an isotropic Adaptive Mesh Refinement (AMR) technique based on the MMG library [39–41] is introduced. The cell size Δx is thus controlled using a criterion based on the gradient of the liquid ammonia mass fraction $\nabla Y_{\mathrm{NH_3},l}$:

$$\Delta x = \min\left(\max\left(\frac{1}{N_{\Delta x}|\nabla Y_{\mathrm{NH_3},l}|}, \Delta x_{min}\right), \Delta x_{init}\right) \tag{46}$$

where $N_{\Delta x} = 20$ refers to the number of cells in the gradient and $\Delta x_{min} = 0.1$ mm is the minimum authorized cell size. The latter parameter limits the cell size in case of too strong local gradient. In addition, the growthrate is limited to 1.05 to prevent excessive cell size variation due to violent gradient. The mesh is adapted every 1000 iterations of the flow solver. Note that this parameter was chosen arbitrarily, but it was found to be sufficient to ensure satisfactory discretisation of the gradients. Starting from 220 000 triangles, the number of elements increases as the spray spreads and reaches, for example, 838 000 after $t = 1.7$ ms of simulation time. Figure 14 shows the field of element sizes at this simulation time.

5.2. Results

Figure 15 gives the result of the simulation after $t = 1.7$ ms. For ease of reading, only the area of interest bounded by the dots and labelled 'Zoom' in Fig. 13 is shown. All the expected physical phenomena are well reproduced. The leak from the tank creates a two-phase jet of ammonia that propagates

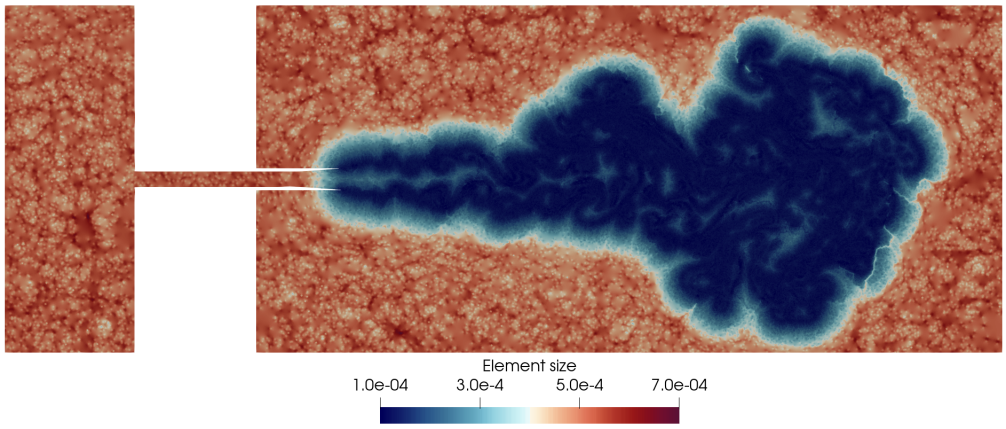

Figure 14: Element size field at $t = 1.7$ ms in the "Zoom" region (see Fig. 13) of the 2D simulation of a two-phase jet from a leaking tank.

through the domain at high speed. Evaporation of the ammonia begins in the leak channel, causing the density of the jet to drop rapidly. The local expansion then accelerates the jet, which leaves the channel at a very high speed, creating shocks. These can be seen in Fig. 16, which shows a density-based numerical schlieren defined as [42]:

$$\zeta = \exp\left(-k\frac{|\nabla\rho|}{\max(|\nabla\rho|)}\right) \tag{47}$$

with $k = 100$. On contact with the cold jet, the water contained in the humid air at rest condenses in the shear zone. It then mixes with the ammonia, creating a downstream spray consisting of a two-phase mixture of liquid and gaseous ammonia, liquid and vapor water and air, which spreads into the atmosphere.

All the expected physical phenomena are therefore well represented, demonstrating the relevance and robustness of the present strategy for simulating

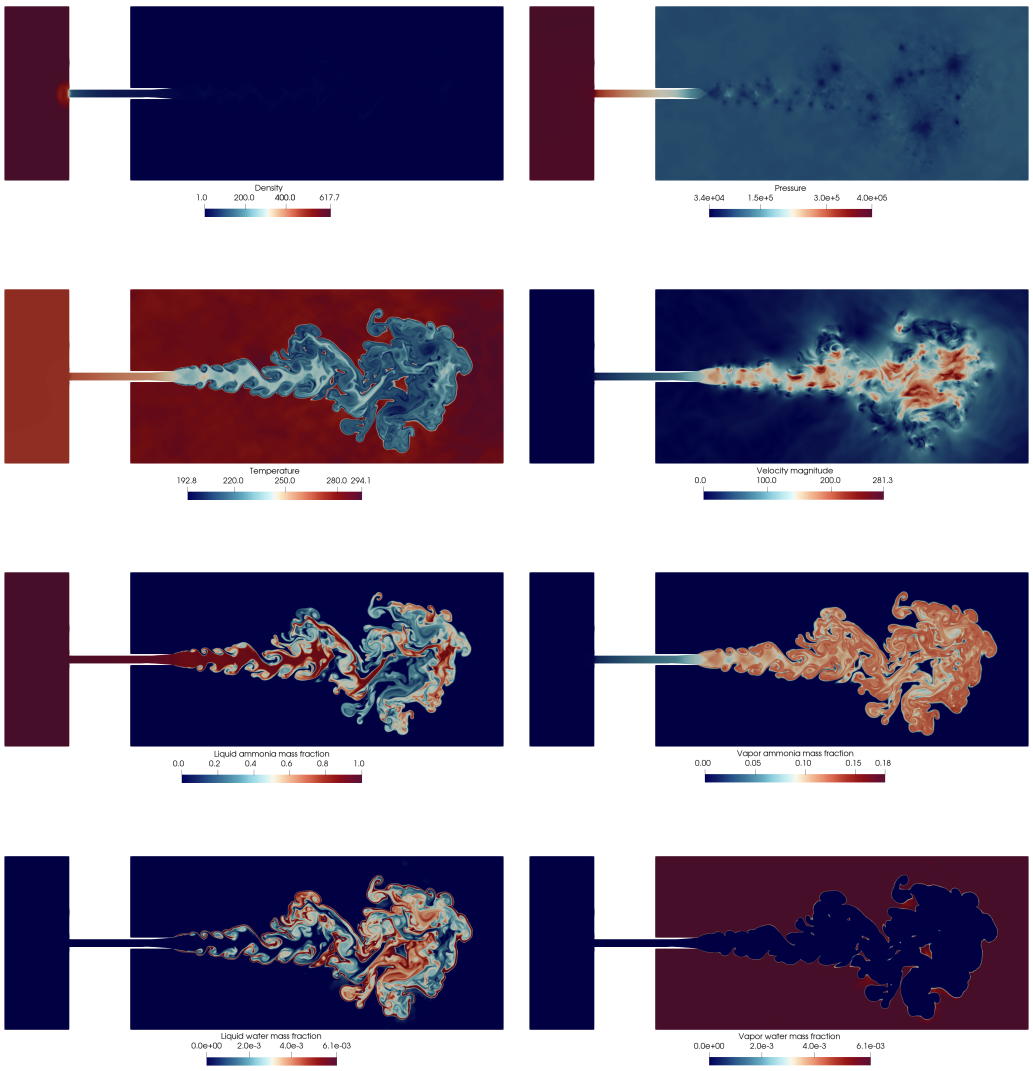

Figure 15: Fields of density, pressure, temperature, velocity magnitude and mass fractions at $t = 1.7$ ms in the 'zoom' region (see Fig. 13) of the 2D simulation of a two-phase jet from a leaking tank.

pressurised liquefied gas leaks. In particular, this will allow to investigate the safety risks associated with ignition of the mixture and the influence of

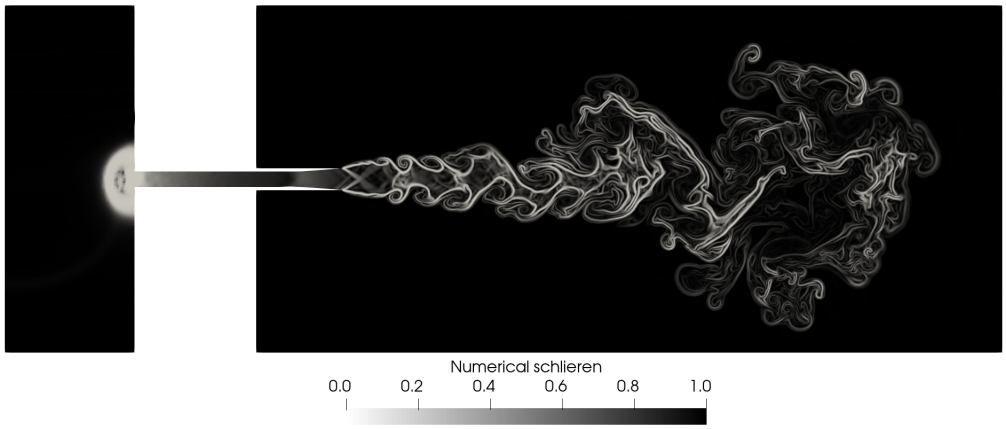

Figure 16: Numerical schlieren field at $t = 1.7$ ms in the "Zoom" region (see Fig. 13) of the 2D simulation of a two-phase jet from a leaking tank.

humidity on these risks in a future work.

6. Concluding remarks

We have presented:

- a new explicit thermodynamic closure for mixtures of two liquid-vapor couples and an arbitrary number of non-condensable gases.
- a rapid Vapor-Liquid Equilibrium (VLE) solver for the said mixture, to be used in numerical simulations.

The resulting framework was validated via a series of shock-tube simulations, systematically testing the models under extreme conditions, and exploring the pure liquid and pure gas limits, where the vapor-liquid equilibrium no longer exists.

The robustness of the approach was also shown via a complex two-dimensional simulation of an ammonia leak. In future work, the model will be tested in configurations relevant for the safety of cryogenic H_2 tanks.

Acknowledgements

The authors would like to thank J. Qufaj for his preliminary work on the model during his internship at the M2P2 laboratory. This project was provided with computer and storage resources by GENCI at TGCC thanks to the grant 2023-A0152B06880 on the supercomputer Joliot Curie's the ROME partition and to CRIANN resources under the allocation 2012006.

References

[1] P. Boivin, M. Le Boursicaud, A. Millan-Merino, S. Taileb, J. Melguizo-Gavilanes, F. A. Williams, Hydrogen ignition and safety, in: Hydrogen for future thermal engines, Springer, 2023.

[2] H. Kobayashi, A. Hayakawa, K. K. A. Somarathne, E. C. Okafor, Science and technology of ammonia combustion, Proceedings of the combustion institute 37 (1) (2019) 109–133.

[3] G. Ariemma, P. Sabia, G. Sorrentino, P. Bozza, M. De Joannon, R. Ragucci, Influence of water addition on mild ammonia combustion performances and emissions, Proceedings of the combustion Institute 38 (4) (2021) 5147–5154.

[4] Q. Zhang, Z. Zhou, S. Shan, X. Cai, W. Yang, Chemical effect of water addition on the ammonia combustion reaction, Thermal Science and Engineering Progress 32 (2022) 101318.

[5] J. M. Prausnitz, R. N. Lichtenthaler, E. Gomes de Azevedo, Molecular Thermodynamics of Fluid-Phase Equilibria, 3rd Edition, PH PTR, 1999.

[6] H. Zhang, S. Yang, Numerical investigation of high-pressure transcritical shock-droplet interaction and mixing layer using vle-based cfd accelerated by isat, in: AIAA SCITECH 2023 Forum, 2023, p. 1857.

[7] P. Downar-Zapolski, Z. Bilicki, L. Bolle, J. Franco, The non-equilibrium relaxation model for one-dimensional flashing liquid flow, International Journal of Multiphase Flow 22 (3) (1996) 473–483. doi:https://doi.org/10.1016/0301-9322(95)00078-X.

[8] E. Faucher, J.-M. Hénard, M. Barret, C. Toulemonde, Computation of flashing flows in variable cross-section ducts, International Journal of Computational Fluid Dynamics 13 (4) (2000) 365–391. doi:https://doi.org/10.1080/10618560008940907.

[9] A. Zein, M. Hantke, G. Warnecke, Modeling phase transition for compressible two-phase flows applied to metastable liquids, Journal of Computational Physics 229 (8) (2010) 2964–2998. doi:https://doi.org/10.1016/j.jcp.2009.12.026.

[10] H. Lund, P. Aursand, Two-phase flow of co2 with phase transfer, Energy Procedia 23 (2012) 246–255, the 6th Trondheim Conference on CO2 Capture, Transport and Storage. doi:https://doi.org/10.1016/j.egypro.2012.06.034.

[11] A. Chiapolino, P. Boivin, R. Saurel, A simple and fast phase transi-

tion relaxation solver for compressible multicomponent two-phase flows, Computers & Fluids 150 (2017) 31–45.

[12] M. De Lorenzo, P. Lafon, M. Di Matteo, M. Pelanti, J.-M. Seynhaeve, Y. Bartosiewicz, Homogeneous two-phase flow models and accurate steam-water table look-up method for fast transient simulations, International Journal of Multiphase Flow 95 (2017) 199–219. doi:https://doi.org/10.1016/j.ijmultiphaseflow.2017.06.001.

[13] M. Pelanti, Arbitrary-rate relaxation techniques for the numerical modeling of compressible two-phase flows with heat and mass transfer, International Journal of Multiphase Flow 153 (2022) 104097. doi:https://doi.org/10.1016/j.ijmultiphaseflow.2022.104097.

[14] S. Le Martelot, R. Saurel, B. Nkonga, Towards the direct numerical simulation of nucleate boiling flows, International Journal of Multiphase Flow 66 (2014) 62–78. doi:https://doi.org/10.1016/j.ijmultiphaseflow.2014.06.010.

[15] R. Saurel, P. Boivin, O. Le Métayer, A general formulation for cavitating, boiling and evaporating flows, Computers & Fluids 128 (2016) 53–64.

[16] X. Deng, P. Boivin, Diffuse interface modelling of reactive multi-phase flows applied to a sub-critical cryogenic jet, Applied Mathematical Modelling 84 (2020) 405–424. doi:https://doi.org/10.1016/j.apm.2020.04.011.

[17] A. D. Demou, N. Scapin, M. Pelanti, L. Brandt, A pressure-based diffuse interface method for low-mach multiphase flows with mass transfer, Journal of Computational Physics 448 (2022) 110730. doi:https://doi.org/10.1016/j.jcp.2021.110730.

[18] B. Peden, J. Carmona, P. Boivin, T. Schmitt, B. Cuenot, N. Odier, Numerical assessment of diffuse-interface method for air-assisted liquid sheet simulation, Computers & Fluids 266 (2023) 106022. doi:https://doi.org/10.1016/j.compfluid.2023.106022.

[19] M. Baer, J. Nunziato, A two-phase mixture theory for the deflagration-to-detonation transition (DDT) in reactive granular materials, International Journal of Multiphase Flow 12 (6) (1986) 861–889.

[20] P. Boivin, M. Cannac, O. Le Métayer, A thermodynamic closure for the simulation of multiphase reactive flows, International Journal of Thermal Sciences 137 (2019) 640–649.

[21] O. Le Métayer, R. Saurel, The noble-abel stiffened-gas equation of state, Physics of Fluids (1994-present) 28 (4) (2016) 046102.

[22] A. Chiapolino, P. Boivin, R. Saurel, A simple phase transition relaxation solver for liquid–vapor flows, International Journal for Numerical Methods in Fluids 83 (7) (2017) 583–605, fld.4282.

[23] D. Furfaro, R. Saurel, Modeling droplet phase change in the presence of a multi-component gas mixture, Applied Mathematics and Computation 272 (2016) 518–541.

[24] R. Saurel, F. Petitpas, R. Abgrall, et al., Modelling phase transition in metastable liquids: application to cavitating and flashing flows, Journal of Fluid Mechanics 607 (1) (2008) 313–350.

[25] R. Saurel, F. Petitpas, R. A. Berry, Simple and efficient relaxation methods for interfaces separating compressible fluids, cavitating flows and shocks in multiphase mixtures, Journal of Computational Physics 228 (5) (2009) 1678–1712.

[26] O. Le Métayer, J. Massoni, R. Saurel, Dynamic relaxation processes in compressible multiphase flows. application to evaporation phenomena, in: ESAIM:Proc., 2013, pp. 103–123. doi:https://doi.org/10.1051/proc/201340007.

[27] S. H. R. Syed, A. H. Robert, Vapor-liquid equilibria in the ammonia-water system, Journal of Chemical & Engineering Data 32 (1987) 183–191. doi:https://doi.org/10.1021/je00048a017.

[28] G. M. G. Muller, E. Bender, Berichte der Bunsengesellschaft f́ur physikalische Chemie 92 (1988) 148–160. doi:https://doi.org/10.1002/bbpc.198800036.

[29] H. R. J.L. Guillevic, D. Richon, Vapor-liquid equilibrium data for the binary system water-ammonia at 403.1, 453.1, and 503.1 k up to 7.0 mpa, Journal of Chemical and Engineering Data 30 (1985) 332–335. doi:https://doi.org/10.1021/je00041a030.

[30] S. O. C.D. Holcomb, Near-saturation (p,ρ,t) and vapor-pressure measurements of nh3, and liquid-phase isothermal (p,ρ,t) and bubble-point-

pressure measurements of nh3+h2o mixtures, Fluid Phase Equilibria 164 (1999) 97–106. doi:https://doi.org/10.1016/S0378-3812(99)00242-3.

[31] U. K. C. on the Properties of Steam, UK Steam Tables in SI Units, Edward Arnold (Publishers), 1970.

[32] C.-T. Liu, W. Lindsay, Vapor pressure of deuterated water from 106 to 300.deg., Journal of Chemical Engineering Data 15 (1970) 510–513. doi:https://doi.org/10.1021/je60047a015.

[33] N. Vargaftik, Tables on the thermophysical properties of liquids and gases : in normal and dissociated states, Washington : Hemisphere Pub. Corp. ; New York : distributed by Halsted Press, 1975.

[34] T. Poinsot, S. Lele, Boundary conditions for direct simulations of compressible viscous flows, Journal of Computational Physics 101 (1) (1992) 104–129. doi:https://doi.org/10.1016/0021-9991(92)90046-2.

[35] V. Moureau, D. Pascale, L. Vervisch, Design of a massively parallel cfd code for complex geometries, Comptes Rendus Mecanique 339 (2) (2011) 141–148, high Performance Computing. doi:https://doi.org/10.1016/j.crme.2010.12.001.
URL https://www.sciencedirect.com/science/article/pii/S1631072110002111

[36] P.-H. Cournède, B. Koobus, A. Dervieux, Positivity statements for a mixed-element-volume scheme on fixed and moving grids, European

Journal of Computational Mechanics/Revue Européenne de Mécanique Numérique 15 (7-8) (2006) 767–798.

[37] E. Shima, K. Kitamura, Parameter-free simple low-dissipation ausm-family scheme for all speeds, AIAA Journal 49 (8) (2011) 1693–1709. doi:https://doi.org/10.2514/1.J050905.

[38] K. Kitamuran, E. Shima, Towards shock-stable and accurate hypersonic heating computations: A new pressure flux for ausm-family schemes, Journal of Computational Physics 245 (2013) 62–83. doi:https://doi.org/10.1016/j.jcp.2013.02.046.

[39] C. Dapogny, C. Dobrzynski, P. Frey, Three-dimensional adaptive domain remeshing, implicit domain meshing, and applications to free and moving boundary problems, Tech. rep. (2013).

[40] C. Dobrzynski, P. Frey, Anisotropic delaunay mesh adaptation for unsteady simulations, in: 17th international Meshing Roundtable, United States, 2008, pp. 177–194.

[41] P. Benard, G. Balarac, V. Moureau, , C. Dobrzynski, G. Lartigue, Y. d'Angelo, Mesh adaptation for large-eddy simulations in complex geometries, International journal for numerical methods in fluids 81 (12) (2016) 719–740.

[42] R. K. Shukla, C. Pantano, J. B. Freund, An interface capturing method for the simulation of multi-phase compressible flows, Journal of Computational Physics 229 (19) (2010) 7411–7439. doi:https://doi.org/10.1016/j.jcp.2010.06.025.

Appendix A. Thermodynamic parameters

	$NH_{3(l)}$	$NH_{3(g)}$
C_p [J/kg/K]	4.4467×10^3	2.2343×10^3
γ [−]	2.5074	1.2796
b [m^3/kg]	4.4643×10^{-4}	0
p_∞ [Pa]	$6.178\,955\,506\,090 \times 10^8$	0
q [J/kg]	$-8.646\,478\,030 \times 10^5$	$1.010\,565\,997\,5 \times 10^6$

	$H_2O_{(l)}$	$H_2O_{(g)}$
C_p [J/kg/K]	4.185×10^3	1.908×10^3
γ [−]	1.0123	1.3281
b [m^3/kg]	9.203×10^{-4}	0
p_∞ [Pa]	$1.835\,000\,00 \times 10^8$	0
q [J/kg]	$-1.143\,000 \times 10^6$	$1.957\,000 \times 10^6$

	$N_{2(g)}$
C_p [J/kg/K]	1.045×10^3
γ [−]	1.407
b [m^3/kg]	0
p_∞ [Pa]	0
q [J/kg]	-2.355×10^3

Table A.3: Parameters in SI units for liquid and gaseous ammonia and water and gaseous nitrogen derived using the methodology of [20].

Appendix B. Determination of bubble and dew points pressures and temperatures from the Rachford-Rice equation

By definition, the bubble and dew points correspond respectively to temperature at given pressure - or inversely pressure at given temperature - where the first bubble of vapor and the first droplet of liquid are formed. In practice, they relate to the solution of the Rachford-Rice Eq. (18) with $\tau_g = 0$ and $\tau_g = 1$, respectively.

The bubble point pressure p_{bubble}, or temperature T_{bubble}, for a binary mixture of two condensable components can be obtained from the simplified

Rachford-Rice Eq. (20), by setting $\tau_g = 0$:

$$(K_1 - 1)z_1 + (K_2 - 1)z_2 = 0 \tag{B.1}$$

Taking into account the expression of K_k and noting that, since $\tau_g = 0$, then $z_k = X_{k,l}$, this equation can be reformulated as:

$$z_1 p_{sat,1}(T) a_1(T, z_1)\, \mathcal{P}_1(p, T) + z_2 p_{sat,2}(T) a_2(T, z_2)\, \mathcal{P}_2(p, T) = p \tag{B.2}$$

where $p_{sat,k}$ depends on temperature through the Antoine equation (see Sec. 3.3). Thus, at a fixed pressure p and mixture composition, the bubble point temperature T_{bubble} can be obtained by solving Eq. (B.2) through a simple Newton-Raphson algorithm. The bubble point pressure p_{bubble} can be determined in the same way, but by fixing the temperature T. Note that, if the Poynting factor $\mathcal{P}_k(p, T)$ is neglected, the bubble point pressure p_{bubble} is obtained explicitly from Eq. (B.2).

The dew point pressure p_{dew}, or temperature T_{dew}, can be obtained similarly by setting $\tau_g = 1$ in the Rachford-Rice Eq. (20):

$$\frac{z_1}{K_1} + \frac{z_2}{K_2} = 1 \tag{B.3}$$

which can be reformulated as previously as:

$$\frac{z_1}{p_{sat,1}(T) a_1(T, X_{1,l})\, \mathcal{P}_1(p, T)} + \frac{z_2}{p_{sat,2}(T) a_2(T, X_{2,l})\, \mathcal{P}_2(p, T)} = \frac{1}{p} \tag{B.4}$$

Here again, using this equation, the dew point pressure p_{dew} can be calculated by fixing the temperature T or, alternatively the dew temperature T_{dew} can be determined for a given pressure p. However, even if the Poynting factor $\mathcal{P}_k(p, T)$ is ignored, the dew point pressure p_{dew} still cannot be obtained

explicitly because the mole fraction of components $k = 1, 2$ in the liquid phase $X_{k,l}$ required to calculate the activity coefficients is not known. A simple iterative methodology is thus used. The pressure is first calculated by Eq. B.4 assuming that $a_1(T, X_{1,l}) = 1$ and $a_1(T, X_{2,l}) = 1$. The mole fractions $X_{k,l}$ are then computed by combining expressions of the equilibrium constant Eqs. (29) and (31) (or Eqs. (30) and (32)):

$$X_{k,l} = \frac{z_k P}{p_{sat,k}(T) a_k(T, X_{k,l}) \mathcal{P}_k(p, T)} \tag{B.5}$$

with $z_k = X_{k,g}$ because $\tau_g = 1$. They are finally used to recompute the activity coefficients and dew point pressure. The full procedure is repeated until the convergence of mole fraction values is reached.

In the case of a complex mixture including two condensable components and several non-condensable gas ($\forall k \geq 3$, $z_{k,g} > 0$), the bubble point disappears as discussed in Sec. 3.4. This is clearly illustrated by the fact that $\tau_g = 0$ is a forbidden value of Eq. (20). On the other hand, the dew point pressure p_{dew}, or temperature T_{dew}, can be obtained from Eq. (B.4) previously derived for the binary mixture but considering that $z_1 + z_2 + \sum_{k\geq 3}^{N} z_k = 1$ instead of $z_1 + z_2 = 1$.

Appendix C. Summary of the Newton-Rachford algorithm for equilibrium at given (ρ, e)

The method to solve directly the algebraic system (45) is presented here. Eliminating condensable mass fractions by τ_g using Eq. (43), the system (45)

becomes:

$$\begin{cases} v = & \sum_{k=1,2} z_k \frac{W_k}{\overline{W}\left[1+(K_k-1)\tau_g^*\right]} \left[\left(1-\tau_g^*\right) v_{k,l}(T^*,p^*) \right. \\ & \left. +K_k\tau_g^* v_{k,g}(T^*,p^*)\right] + \sum_{k=3}^{N} Y_{k,g} v_{k,g}(T^*,p^*) \\ e = & \sum_{k=1,2} z_k \frac{W_k}{\overline{W}\left[1+(K_k-1)\tau_g^*\right]} \left[\left(1-\tau_g^*\right) e_{k,l}(T^*,p^*) \right. \\ & \left. +K_k\tau_g^* e_{k,g}(T^*,p^*)\right] + \sum_{k=3}^{N} Y_{k,g} e_{k,g}(T^*,p^*) \\ & \frac{(K_1-1)z_1}{1+(K_1-1)\tau_g^*} + \frac{(K_2-1)z_2}{1+(K_2-1)\tau_g^*} + \sum_{k=3}^{N} \frac{z_k}{\tau_g^*} = 0 \end{cases} \tag{C.1}$$

In order to solve this system (C.1), it is rewritten as:

$$\begin{cases} f_1(p^*,T^*,\tau_g^*) = & v - \sum_{k=1,2} z_k \frac{W_k}{\overline{W}\left[1+(K_k-1)\tau_g^*\right]} \left[\left(1-\tau_g^*\right) v_{k,l}(T^*,p^*) \right. \\ & \left. +K_k\tau_g^* v_{k,g}(T^*,p^*)\right] + \sum_{k=3}^{N} Y_{k,g} v_{k,g}(T^*,p^*) \\ f_2(p^*,T^*,\tau_g^*) = & e - \sum_{k=1,2} z_k \frac{W_k}{\overline{W}\left[1+(K_k-1)\tau_g^*\right]} \left[\left(1-\tau_g^*\right) e_{k,l}(T^*,p^*) \right. \\ & \left. +K_k\tau_g^* e_{k,g}(T^*,p^*)\right] + \sum_{k=3}^{N} Y_{k,g} e_{k,g}(T^*,p^*) \\ f_3(p^*,T^*,\tau_g^*) = & \frac{(K_1-1)z_1}{1+(K_1-1)\tau_g^*} + \frac{(K_2-1)z_2}{1+(K_2-1)\tau_g^*} + \sum_{k=3}^{N} \frac{z_k}{\tau_g^*} \end{cases} \tag{C.2}$$

As the algebraic system (C.2) is non-linear, it is common to use an iterative method such as a Newton-Raphson's algorithm (also simply called Newton's algorithm). Let's then define:

$$\mathbf{X} = \begin{bmatrix} p^* \\ T^* \\ \tau_g^* \end{bmatrix} \tag{C.3}$$

and,

$$F(\mathbf{X}) = \begin{bmatrix} f_1(p^*,T^*,\tau_g^*) \\ f_2(p^*,T^*,\tau_g^*) \\ f_3(p^*,T^*,\tau_g^*) \end{bmatrix}. \tag{C.4}$$

The system is resolved when $F(\mathbf{X}) = \mathbf{0}$. Its solution vector $\mathbf{X}$ is expressed as:

$$\mathbf{X}^n = \mathbf{X}^{n-1} - \left(\frac{\partial \mathbf{F}}{\partial \mathbf{X}}\right)^{-1} F(\mathbf{X}^{n-1}) \tag{C.5}$$

where n denotes the current iteration of the iterative method and, $\frac{\partial \mathbf{F}}{\partial \mathbf{X}}$ is the Jacobian matrix:

$$\frac{\partial \mathbf{F}}{\partial \mathbf{X}} = \begin{bmatrix} \frac{\partial f_1}{\partial p^*} & \frac{\partial f_1}{\partial T^*} & \frac{\partial f_1}{\partial \tau_g^*} \\ \frac{\partial f_2}{\partial p^*} & \frac{\partial f_2}{\partial T^*} & \frac{\partial f_2}{\partial \tau_g^*} \\ \frac{\partial f_3}{\partial p^*} & \frac{\partial f_3}{\partial T^*} & \frac{\partial f_3}{\partial \tau_g^*} \end{bmatrix}. \tag{C.6}$$

Following the Newton-Raphson's algorithm, the equation (C.5) can be iterated until convergence of $\mathbf{X}$ is reached. This convergence is obtained when:

$$\epsilon = \sqrt{\frac{1}{3}\sum_{i=1}^{3}\left[\left(X_i^n - X_i^{n-1}\right)\cdot W_i\right]^2} < 1 \tag{C.7}$$

where $\mathbf{W}$ is a vector containing the weights computed as follows:

$$\forall\, \mathrm{i} = 1...3,\, W_i = \left(r_{tol,i}|X_i^n| + a_{tol,i}\right)^{-1}. \tag{C.8}$$

$\mathbf{r}_{tol}$ and $\mathbf{a}_{tol}$ are respectively vectors containing the relative and absolute tolerance on error for each variable. Their values are set to:

$$\forall\, \mathrm{i} = 1...3,\, r_{tol,i} = 10^{-6} \tag{C.9}$$

and,

$$\mathbf{a}_{tol} = \begin{bmatrix} 10^{-2}\ \mathrm{Pa} \\ 10^{-2}\ \mathrm{K} \\ 10^{-14} \end{bmatrix}. \tag{C.10}$$